

A simple model of ultrasound propagation in a cavitating liquid. Part I: Theory, nonlinear attenuation and traveling wave generation.

O. Louisnard^{a,*}

^a*Centre RAPSODEE, FRE CNRS 3213, Université de Toulouse, Ecole des Mines d'Albi, 81013 Albi Cedex 09, France*

Abstract

The bubbles involved in sonochemistry and other applications of cavitation oscillate inertially. A correct estimation of the wave attenuation in such bubbly media requires a realistic estimation of the power dissipated by the oscillation of each bubble, by thermal diffusion in the gas and viscous friction in the liquid. Both quantities are calculated numerically for a single inertial bubble driven at 20 kHz, and are found to be several orders of magnitude larger than the linear prediction. Viscous dissipation is found to be the predominant cause of energy loss for bubbles small enough. Then, the classical nonlinear Caflish equations describing the propagation of acoustic waves in a bubbly liquid are recast and simplified conveniently. The main harmonic part of the sound field is found to fulfill a nonlinear Helmholtz equation, where the imaginary part of the squared wave number is directly correlated with the energy lost by a single bubble. For low acoustic driving, linear theory is recovered, but for larger drivings, namely above the Blake threshold, the attenuation coefficient is found to be more than 3 orders of magnitude larger than the linear prediction. A huge attenuation of the wave is thus expected in regions where inertial bubbles are present, which is confirmed by numerical simulations of the nonlinear Helmholtz equation in a 1D standing wave configuration. The expected strong attenuation is not only observed but furthermore, the examination of the phase between the pressure field and its gradient clearly demonstrates that a traveling wave appears in the medium.

Keywords: Acoustic cavitation, Bubble dynamics, Propagation in bubbly liquids, Wave attenuation

PACS: 43.25.Yw, 43.35.Ei, 43.25.Gf

1. Introduction

The complexity and large variety of spatial and temporal scales involved in acoustic cavitation make difficult the derivation of a full theoretical model, accounting for the coupled effects between the bubble field and the sound field. Nevertheless, considerable progress has been made in the last decade. Theoretical studies in the context of single bubble sonoluminescence have allowed to restrict the ambient size of the bubbles in the micron range, owing to surface instabilities [1–7]. This has been confirmed by 20 kHz experiments, both in single bubble [8] and multi-bubble configurations (see Ref. [9] and references therein).

Besides, a large collection of experimental observations have revealed that radially oscillating bubbles in high-intensity acoustic fields tend to self-organize into bubble structures, which shapes depend on the experimental configuration, with possibly two structures or more appearing simultaneously in different zones of the liquid [9–13]. The shape of such structures is strongly correlated with the fundamental issue of the translational motion of the bubbles under Bjerknes forces, which have been reconsidered

in the context of strongly nonlinear inertial radial oscillations and traveling waves [7, 14, 15].

On this basis, the action of the acoustic field on the organization of inertial bubbles has been satisfactorily described in various configurations by particle models [7, 10, 13, 16], by calculating the forces exerted on the bubbles directly from their nonlinear dynamics. Assuming a simple shape of the sound field, some bubble structures have been remarkably caught by this method. However, the correct prediction of other structures was found to be more difficult, mainly because, as suggested by Mettin [9], the local sound field might have a complicated shape, which cannot be inferred without describing correctly the acoustic field in the medium.

The backward effect of inertial bubbles on the propagation of acoustic waves remains mainly unexplored. The main physical effects of the bubble radial oscillations on sound waves can be easily understood qualitatively. Bubbles are mechanical oscillators so that wave dispersion is expected. They oscillate non linearly for large amplitude drivings, so that waves should be nonlinear. Finally, they dissipate mechanical energy by various processes, which should produce wave attenuation. The problem has been attacked in the early work of Foldy [17] who considered linear scattering of waves by an arbitrary statistical distribution

*Corresponding author

Email address: louisnar@enstima.fr (O. Louisnard)

bution of scatterers, and obtained a linear dispersion relation. The application of this theory to the specific case of linear sound waves in bubbly liquids has been considered in Refs. [18, 19]. A key feature in Foldy’s approach is that for a sufficiently dilute bubbly mixture, each bubble behaves as if it were excited by the statistical average pressure field, which allows to cast aside the difficult issue of bubbles pairwise interaction. An intuitive justification of this approach can be found in Refs. [20, 21].

The assumption of small amplitude waves has been relaxed by Iordansky [22] and simultaneously by van Wijngaarden [23, 24] by a semi-empirical volume-averaging of the bubbly liquid equations, which is closed by a Rayleigh equation, where, as suggested by Foldy’s work, the driving pressure term is the local average pressure field. The model obtained has allowed the study of nonlinear dispersive waves. The latter are classically described by the Korteweg-de Vries equation [25], and the reduction of van Wijngaarden model to the latter for moderate amplitudes has been studied by various authors both theoretically [24, 26–28] and experimentally [29–31].

The popular Caffish model [32] is a rigorous generalization of Foldy’s theory to the nonlinear case and yields a simplified version of van Wijngaarden model, as far as the bubbly liquid is dilute enough. The latter hypothesis has the important corollary that the mean velocity of the mixture is infinitely small, so that the momentum conservation equation coincide with the one of linear acoustics [see Eq. (2) below]. A physical discussion of the latter feature can be found in Refs. [20, 21].

Under the linear approximation, the Caffish model reduces to the famous dispersion relation of Foldy, which can be extended to calculate a wave attenuation coefficient, accounting for dissipation by a linearly oscillating bubble [20] and to polydisperse bubbles size distributions. Linearization allows a simple description of the sound field by an Helmholtz equation, and has been used in studies of the coupling between wave propagation and the bubble field. The gain obtained by simplifying the wave equation allows a complex description of its coupling with the bubble population evolution, spatially and along the size axis. Following such an approach, Kobelev & Ostrovski [33] have proposed an elegant model of self-action of low amplitude sound waves in bubbly liquids, accounting for the bubble drift under the action of primary Bjerknes forces and bubble coalescence favored by secondary Bjerknes forces. Although the wave equation in this study was linear, the global model was nonlinear, owing to the dependence of the wave number on the varying bubble density, which conversely evolves non linearly with the sound field. Specific solutions under different hypothesis could catch the experimentally observed self-transparency, self-focusing of sound waves in bubbly liquids, and destabilization of homogeneous bubble distributions. The latter instability has also been demonstrated in Ref. [34] by a similar approach, but involving a slightly different physics.

The attenuation of sound waves by oscillating bubbles

remains normally weak for linear waves, except when the bubbles are close to the resonant size [17, 20, 35], which is the main cause of sound extinction considered in Ref. [33]. Since low-frequency inertial cavitation involves bubbles much smaller than the resonant size [9], the use of the linear theory of Ref. [20] predicts an abnormally low attenuation, compared to experimental data [36]. This is not astonishing since inertial bubbles typically suffer a ten-fold expansion of their radius and are expected to dissipate more energy than predicted by linear theory. Despite the latter restriction, the linear dispersion relation has often been used to predict attenuation of strong cavitation fields, because it allows the description of the problem by a linear Helmholtz equation, which is easy to solve, and allows harmonic response simulations [37–40]. Moreover, the use of a complex wave number provided by the linear dispersion relation in an Helmholtz equation somewhat masks the fact that one physical origin of wave attenuation by the bubbles is the energy dissipated by the latter. The latter point has been nicely addressed by Rozenberg [41], who restated the problem of attenuation of a traveling wave by a cavitation zone in terms of energy conservation, without resorting to the linear hypothesis. The latter study made use of an empirical expression, fitted on experimental results, between the power dissipated by cavitation bubbles and the wave intensity. Doing so, realistic attenuated intensity profiles near the emitter could be calculated simply, and experimentally observed self-attenuation of the wave could be accounted for.

The last remarks suggests that the relaxation of the linear hypothesis is necessary to correctly predict attenuation by inertial bubbles, so that one should revert to the original fully nonlinear form of the Caffish model. However, although valid for any wave amplitude, the latter remains intractable for large multi-dimensional geometries, since it requires time-dependent simulations, and presents convergence problems in the range of inertial cavitation, even in 1D [42, 43]. Thus, an intermediate model, simple enough to be numerically tractable, but properly accounting for the true energy dissipation by inertial bubbles, is necessary.

The motivation of this work is the derivation of such a reduced model, and can be viewed as a systematic formalization of Rozenberg’s approach [41], based on the nonlinear Caffish model. The present paper extends the ideas formerly presented in Ref. [44] and is organized as follows. In section 2, we recast the fully nonlinear Caffish equations into a mechanical energy balance equation, where we express explicitly the energy lost by the bubbly liquid on average over an oscillation period, as functions of period-averaged quantities of a single bubble dynamics. This energy loss is then computed numerically, by simulating a bubble radial dynamics equation over a typical parameter range, including the range of inertial cavitation involved in cavitation and sonochemistry experiments. In section 3, we then seek a reduction of the Caffish equations for the main harmonic component of the acoustic field, involving

the energy dissipation calculated in section 2. Finally, in section 4, the resulting nonlinear Helmholtz equation is solved numerically in a 1D configuration, and a detailed analysis of the obtained wave profiles is performed. The implications of the present results on the primary Bjerknes forces and 2D simulations of classical experimental configurations are deferred in a companion paper.

2. Theory

2.1. Caffish equations

The Caffish model [32] describes the propagation of an acoustic wave of arbitrary amplitude in a bubbly liquid described as a continuum, which means that the radial oscillations of all the bubbles pertaining to an elementary small volume of mixture located at a spatial point \mathbf{r} can be described by a continuous spatio-temporal radius function $R(\mathbf{r}, t)$. The first two equations of the model correspond to mass and momentum conservation in the mixture:

$$\frac{1}{\rho_l c_l^2} \frac{\partial p}{\partial t} + \nabla \cdot \mathbf{v} = \frac{\partial \beta}{\partial t}, \quad (1)$$

$$\rho_l \frac{\partial \mathbf{v}}{\partial t} + \nabla p = 0. \quad (2)$$

In the above equations, $p(\mathbf{r}, t)$ is the acoustic pressure field, $\mathbf{v}(\mathbf{r}, t)$ the velocity field, ρ_l the liquid density, c_l the sound speed in the liquid, and $\beta(\mathbf{r}, t)$ is the instantaneous void-fraction, which, assuming a mono-disperse distribution of the bubbles, can be defined by:

$$\beta(\mathbf{r}, t) = N(\mathbf{r}) \frac{4}{3} \pi R(\mathbf{r}, t)^3, \quad (3)$$

where $N(\mathbf{r})$ is the local bubble density. The latter is assumed time-independent, or at least almost constant on the time scale of the oscillations. Despite the set of equations (1) and (2) is very similar to the equations of linear acoustics, the presence of the right-hand-side term of Eq. (1) renders the whole model nonlinear. Following the procedure classically used for linear acoustics, these two equations can be easily recast into an equation of energy conservation, by multiplying (1) by p and (2) by \mathbf{v} :

$$\frac{\partial}{\partial t} \left(\frac{1}{2} \frac{p^2}{\rho_l c_l^2} + \frac{1}{2} \rho_l v^2 \right) + \nabla \cdot (p\mathbf{v}) = Np \frac{\partial V}{\partial t}, \quad (4)$$

where $V(\mathbf{r}, t)$ denotes the instantaneous volume of the bubbles located at \mathbf{r} . The time derivative in the left-hand-side (LHS) of this equation represent the time-variations of the acoustic energy density, which is the sum of kinetic energy and potential compressional energy of the pure liquid. The second LHS-term is the divergence of the acoustic intensity $p\mathbf{v}$. The right-hand-side (RHS), which would be zero for a linear wave propagating in the pure liquid, represents the mechanical power exchanged between the acoustic wave and the bubbles. As will be seen below, part of this energy is irreversibly dissipated along the radial oscillations of the bubbles, which is the physical origin of the acoustic wave attenuation.

2.2. Bubble dynamics

The bubble radial motion equation can be described by a radial dynamics equation. The Caffish model in its original form uses a inviscid Rayleigh-Plesset equation with isothermal behavior of the bubble, in which the infinite driving pressure field is the mean local acoustic pressure field $p(\mathbf{r}, t)$. In the present study, we want to examine the energy dissipation by heat transfer between the bubble interior and the liquid, and by viscous friction in the radial motion of the liquid around the bubble. We therefore leave the bubble pressure p_g unspecified for now, and add the classical viscous term in the Rayleigh-Plesset equation. Besides, since surface tension plays a preponderant role in inertial cavitation [45–48], we also added the correction accounting for the latter effect, so that the bubble dynamics is given by:

$$\rho_l \left(R\ddot{R} + \frac{3}{2} \dot{R}^2 \right) = p_g - \frac{2\sigma}{R} - 4\mu_l \frac{\dot{R}}{R} - p, \quad (5)$$

where μ_l is the liquid dynamic viscosity, and σ the surface tension. All the quantities R , p_g and p in this equation are spatio-temporal fields, depending on both \mathbf{r} and t , so that the time derivatives represented by over-dots in this equation must be understood as partial derivatives $\partial/\partial t$ at \mathbf{r} constant. We did not add any corrections accounting for liquid compressibility, in order to keep a reasonably simple model. We defer the discussion of this choice to the conclusion section.

For further use in the paper, we recall that when a bubble is driven by a sinusoidal pressure field $p = p_0 [1 - P^* \sin(2\pi ft)]$ around the ambient pressure p_0 , its oscillations become inertia-controlled and involve a strong collapse when the driving pressure amplitude is above the Blake threshold [45–47]:

$$P_B^* = 1 + \left(\frac{4}{27} \frac{S^3}{1 + S} \right)^{1/2}, \quad (6)$$

where $S = 2\sigma/(p_0 R_0)$ is the dimensionless Laplace tension and R_0 the bubble ambient radius. Such an oscillation regime, historically termed as “transient cavitation”, is now classically named as “inertial cavitation” [5, 49].

2.3. Energy dissipation per bubble

In order to get an energetic interpretation of the bubble radial motion, equation (5) can be multiplied by the time derivative of the bubble volume $\partial V/\partial t$, and noting that $\rho_l(R\ddot{R} + \frac{3}{2}\dot{R}^2) \times \partial V/\partial t$ is the time-derivative of the radial kinetic energy of the liquid $K_l = 2\pi\rho_l R^3 \dot{R}^2$, we obtain:

$$\frac{\partial}{\partial t} (K_l + 4\pi R^2 \sigma) = -16\pi\mu_l R \dot{R}^2 - p \frac{\partial V}{\partial t} + p_g \frac{\partial V}{\partial t}. \quad (7)$$

This equation is strictly equivalent to the Rayleigh equation, and is the expression of the theorem of kinetic energy applied to the liquid surrounding the bubble. The parenthesis in the LHS of (7) represents the sum of the kinetic

energy of the radially moving liquid and the interfacial potential energy.

The first term in the RHS of Eq. (7) is the power irreversibly lost by internal viscous friction within the liquid as it moves radially.

The second term in the RHS is the power transferred from the acoustic field to the liquid surrounding the bubble, and can be viewed as the energy source available to drive the bubble oscillations and the radial motion of the liquid around. When multiplied by the number of bubbles per unit-volume, this term is similar to the right-hand-side of Eq. (4) with the opposite sign, which clearly indicates how energy is transferred between the driving acoustic field and the radially oscillating bubble.

Finally, the last term in the RHS of (7) is the mechanical power done by the gas on the liquid, and could be expressed as the time-derivative of a compressional energy $-\partial E_p/\partial t$ in the case of a barotropic relation between the bubble pressure p_g and volume V (for example assuming an isothermal [32] or adiabatic evolution of the gas). However, in the general case where heat flows irreversibly between the bubble interior and the liquid, this term cannot be expressed as the time-derivative of a potential function, and we now detail how this term is linked to dissipation of energy over a whole oscillation cycle of the bubble.

In what follows, we will assume periodic oscillations of all the fields. Averaging Eq. (7) over one cycle, the time-derivative in the left side cancels and we get:

$$\left\langle -p \frac{\partial V}{\partial t} \right\rangle = \Pi_{\text{th}} + \Pi_{\text{v}}, \quad (8)$$

where the two bubble dynamics-dependent average quantities Π_{th} and Π_{v} read:

$$\Pi_{\text{th}} = \frac{1}{T} \int_0^T -p_g \frac{\partial V}{\partial t} dt, \quad (9)$$

$$\Pi_{\text{v}} = \frac{1}{T} \int_0^T 16\pi\mu_l R \dot{R}^2 dt. \quad (10)$$

The quantity Π_{v} defined by (10) is clearly positive, and is the period-averaged power loss by viscous friction in the liquid.

A clear interpretation of Π_{th} can be obtained by applying the first principle of thermodynamics to the whole bubble content, which yields integral (9) as:

$$\Pi_{\text{th}} = \frac{1}{T} \int_0^T \frac{d(U_g + K_g)}{dt} dt - \frac{1}{T} \int_0^T \dot{Q} dt, \quad (11)$$

where U_g and K_g depict the internal energy and kinetic energy, respectively, of the whole gas in the bubble, and \dot{Q} is the heat gained by the bubble over one cycle. The first integral in the right-hand-side of (11) is zero for a periodic motion, so that $\Pi_{\text{th}} = -\langle \dot{Q} \rangle$ is just the net heat lost by the bubble over one oscillation cycle.

Equation (8) has therefore the following physical meaning: the energy transferred by the acoustic field to the

bubble over one acoustic period is dissipated by two processes: the heat flow from the bubble toward the liquid and the viscous friction in the liquid radial motion.

The integrals Π_{v} and Π_{th} can be evaluated numerically by solving the bubble dynamics equation (5) for an arbitrary single bubble of ambient radius R_0 excited by a sinusoidal forcing $p = p_0 [1 - P^* \sin(2\pi ft)]$, possibly varying the acoustic parameters P^* and f , the bubble ambient radius R_0 , and the properties of the liquid and the gas. In this paper we will restrict to air bubbles in water at ambient pressure excited at 20 kHz and take: $p_0 = 101300$ Pa, $\rho_l = 1000$ kg/m³, $\mu_l = 10^{-3}$ Pa.s, $\sigma = 0.0725$ N.m⁻¹. The bubble ambient radius R_0 and driving pressure amplitude P will be varied within a range of interest. More results involving, among others, the effect of the frequency and the type of gas will be given elsewhere [50].

Since Π_{th} represents the net heat flow leaving the bubble, thermal diffusion in the bubble interior must be properly accounted for in our simulations, at least in an approximate manner. To that aim, the bubble interior is modeled by an approximate energy conservation equation based on a thermal diffusion layer [51–53]. Water evaporation and condensation at the bubble interface is also taken into account by a similar method, as described in the same references. The latter refinement may be important since the presence of water vapor in the bubble is known to decrease the temperature collapse [51] and therefore influences the estimation of \dot{Q} . To solve the bubble radial dynamics, the variables are non-dimensionalized by:

$$t^* = \omega t, \quad R^* = \frac{R}{R_0}, \quad p_g^* = \frac{p_g}{p_0}, \quad \Pi_{\text{v,th}}^* = \frac{\Pi_{\text{v,th}}}{p_0 V_0 \omega},$$

and the dimensionless dissipation functions Π_{th}^* and Π_{v}^* are calculated numerically by:

$$\Pi_{\text{th}}^* = \frac{1}{2\pi} \left(1 + \frac{2\sigma}{p_0 R_0} \right) \int_0^{2\pi} p_g^* \frac{dV^*}{dt^*} dt^*, \quad (12)$$

$$\Pi_{\text{v}}^* = \frac{6}{\pi} \frac{\omega \mu_l}{p_0} \int_0^{2\pi} R^* \left(\frac{dR^*}{dt^*} \right)^2 dt^*. \quad (13)$$

For comparison purposes, we recall that assuming linear oscillations of the bubble, the equation of radial dynamics can be linearized by setting

$$R^*(t) = 1 + \frac{1}{2} \left(X e^{it^*} + \text{c.c.} \right), \quad (14)$$

where the complex amplitude can be obtained analytically, accounting rigorously for thermal effects [28, 54, 55]. Introducing (14) in (15)-(16), Π_{th}^* and Π_{v}^* can be obtained analytically, and we obtain:

$$\Pi_{\text{th,lin}}^* = \frac{3}{2} \left(1 + \frac{2\sigma}{p_0 R_0} \right) \Im(\Phi_g) |X|^2, \quad (15)$$

$$\Pi_{\text{v,lin}}^* = \frac{6\mu_l \omega}{p_0} |X|^2, \quad (16)$$

where Φ_g is a complex dimensionless number which can be expressed in terms of the gas thermal Péclet number

$Pe_{th} = R_0^2 \omega / \chi_g$, where χ_g is the thermal diffusivity of the gas in ambient conditions [55, 56].

Figure 1 displays the values calculated for Π_v^* and Π_{th}^* for an air bubble of ambient radius $R_0 = 3 \mu\text{m}$ driven at 20 kHz in water at ambient pressure and temperature. First, it is seen that the power dissipated either by viscous friction (thick solid line) or by thermal diffusion (thick dashed line) quickly rises in the neighborhood of the Blake threshold (where approximately $\Pi_v^* \simeq \Pi_{th}^* \simeq 1$), well above their value predicted by linear theory (between 5 and 6 orders of magnitude). This clearly demonstrates the need for exact nonlinear bubble dynamics to calculate realistic values of the energy dissipated by inertial bubbles.

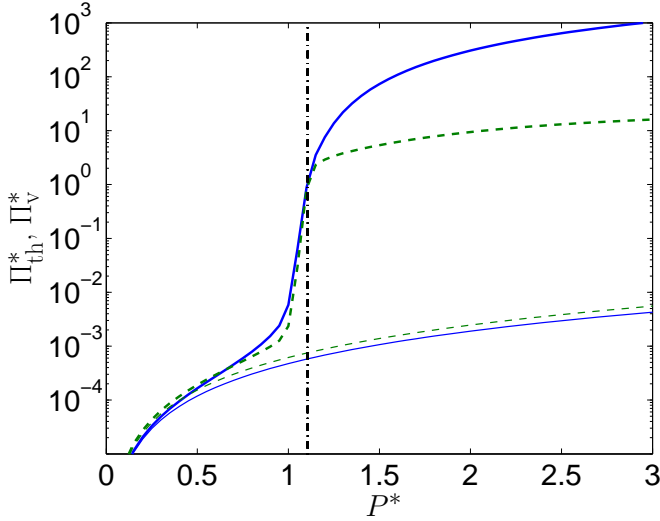


Figure 1: Dimensionless power dissipated by an argon bubble of ambient radius $R_0 = 3 \mu\text{m}$ in water, at 20 kHz: by viscosity Π_v^* [thick solid line, from Eq. (13)]; by thermal diffusion, Π_{th}^* [thick dashed line, from Eq. (12)]. The thin lines are the corresponding values obtained from linear theory, Eqs. (15)-(16) (solid: $\Pi_{v,lin}^*$; dashed: $\Pi_{th,lin}^*$). The vertical dash-dotted line represents the Blake threshold calculated by Eq. (6).

Another interesting feature is that, for the parameters used in Fig. 1, viscous dissipation becomes much larger than the thermal one (more than one order of magnitude), for driving pressures above the Blake threshold, whereas linear theory predicts the opposite in this parameter range. Viscous dissipation in the liquid is thus found to largely predominate over the thermal one for $3 \mu\text{m}$ inertial bubbles.

It is also interesting to interpret these results in the light of the experimental data reported by Rozenberg [41], who fitted the volumic power dissipated in the cavitation zone by the following function of sound intensity I :

$$\mathcal{P} = \begin{cases} A(I - I_t)^2, & I > I_t \\ 0, & I \leq I_t \end{cases}, \quad (17)$$

where I_t is the intensity cavitation threshold. Identifying \mathcal{P} with $N(\Pi_{th} + \Pi_v)$, noting that sound intensity I scales as P^2 for traveling waves, and identifying the cavitation

threshold with Blake threshold, Rozenberg's result suggests that $\Pi_{th} + \Pi_v$ would scale as $P^2 - P_B^2$ for $P > P_B$, and would be 0 under the threshold. This is almost consistent with our results, except that redrawing Fig. 1 with linear scale (not shown) would reveal a linear dependence rather than a quadratic one. However, on one hand, Rozenberg's results apply to 500 kHz fields, and on the other hand, it is highly probable that the bubble density N also depends on the local sound field, despite we will consider N constant above the Blake threshold in the model developed below (see Sec. 4).

We repeated the same calculation for a $8 \mu\text{m}$ bubble (Fig. 2). The scale is chosen identical as Fig. 1 in order to make the comparison easier. The same conclusions apply except that the increase of viscous dissipation Π_v^* over the Blake threshold is lower than for the $3 \mu\text{m}$ bubble, and remains of the same order of magnitude as Π_{th} for moderate driving pressures.

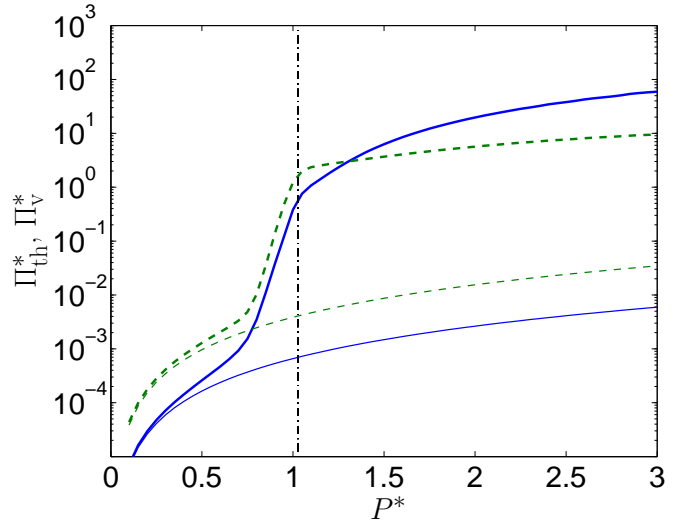


Figure 2: Same as Fig. 1 for a $8 \mu\text{m}$ bubble.

To assess more clearly the dependence of Π_v and Π_{th} on the ambient radius R_0 , we calculated Π_v and Π_{th} at constant $P^* = 1.5$, but varying R_0 . The result is displayed in Fig. 3. Viscous dissipation Π_v is much larger than thermal dissipation Π_{th} just above the Blake threshold, and decreases below Π_{th} only above $R_0 \simeq 10 \mu\text{m}$.

More curves like the ones of Figs. 1, 2 and 3 could be drawn, but we can summarize the comparison of Π_v and Π_{th} above the Blake threshold as follows: Π_v predominates for larger drivings and smaller bubbles, while the opposite is true for larger bubbles and smaller drivings. Since for large drivings, surface instabilities maintain the ambient radii of inertial bubbles in a small interval just above the Blake threshold [1, 3, 57], this suggests that viscous friction would be the predominant dissipation phenomenon in cavitation clouds.

The real power dissipated by an inertial bubble is therefore larger than the one predicted by linear theory by sev-

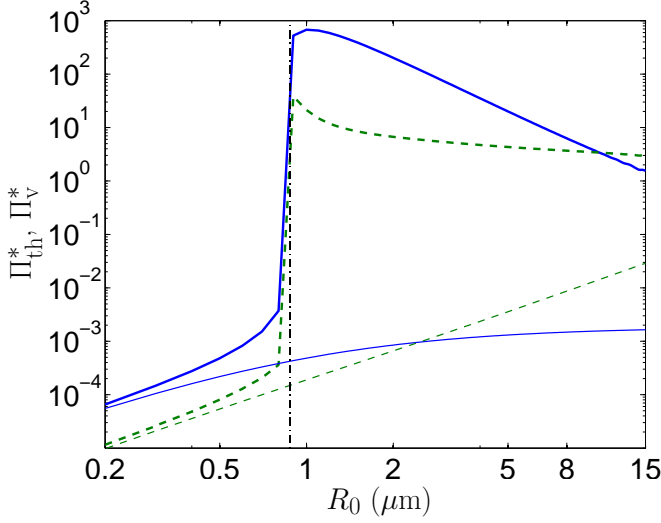


Figure 3: Same as Figs. 1 and 2, but varying R_0 for $P^* = 1.5$. The vertical dash-dotted line represents the Blake threshold.

eral orders of magnitude. We therefore expect the real wave attenuation in a liquid containing inertial bubbles (above the Blake threshold) to be much higher than the value calculated by linear theory. We will quantify this point in Sec. 3.

Although the above results are sufficient to carry on the development of our model, it is instructive to close this section by relating the dissipation functions Π_{th} and Π_v to the conservation of acoustic energy, generalizing the conservation equation proposed in the original paper of Caffish et al. [32].

2.4. Conservation of energy in the bubbly liquid

The term $p\partial V/\partial t$ can be eliminated between equations (4) and (7), by multiplying the latter by N , to obtain a global energy conservation equation of the bubbly liquid:

$$\frac{\partial}{\partial t} \left(\frac{1}{2} \frac{p^2}{\rho_l c_l^2} + \frac{1}{2} \rho_l v^2 + NK_l + 4\pi N \sigma R^2 \right) + \nabla \cdot (p\mathbf{v}) = N p_g \frac{\partial V}{\partial t} - N 16\pi \mu_l R \dot{R}^2. \quad (18)$$

Equation (18) represents the conservation of mechanical energy of the bubbly liquid:

- $p^2/(2\rho_l c_l^2)$ is the elastic potential energy stored by the pure liquid involved in the propagation of the wave,
- $\rho_l v^2/2$ is the kinetic energy per unit volume of the pure liquid involved in the propagation of the wave,
- NK_l is the kinetic energy per unit volume of the liquid in its radial motion around the bubbles,
- $4\pi N \sigma R^2$ is the interfacial potential energy per unit volume,

- $p\mathbf{v}$ is the acoustic intensity, or flux density of mechanical energy. It is supplied at a vibrating boundary in contact with the bubbly liquid, typically by the oscillating motion of the sonotrode [58].

In what follows, we will assume periodic oscillations of all the fields. Averaging Eq. (18) over one cycle, the time-derivative in the left side cancels and we get:

$$\nabla \cdot \langle p\mathbf{v} \rangle = -N (\Pi_{th} + \Pi_v). \quad (19)$$

Equation (19) is the conservation of mechanical energy averaged over one period of oscillation, and has a clear physical interpretation: the balance between the acoustic energy leaving a volume of bubbly liquid and the one reaching it is always negative, owing to thermal loss in the bubble and viscous friction in the radially moving liquid. Each bubble therefore appears as a dissipator of acoustic energy, owing to these two phenomena. The physical origin of wave attenuation is thus self-contained in the Caffish model, even for nonlinear oscillations, provided that a correct model is used to describe thermal diffusion in the bubble interior. Caffish and co-workers proposed a conservation equation similar to (18), disregarding viscosity and assuming isothermal oscillations, in which case mechanical energy is conserved [32]. It should also be noted that Eq. (19) reverts exactly the equation solved in 1D by Rozenberg [41] in the case of purely traveling waves, but in the latter work, the dissipated power was fitted from experimental data, rather than being calculated ab initio from single bubble dynamics as done in the present work.

3. The model

3.1. Intuitive approach

We first recall that the velocity field can be eliminated between Eq. (1) and (2) to yield an equation involving only the pressure field [20, 32]:

$$\nabla^2 p = \frac{1}{c_l^2} \frac{\partial^2 p}{\partial t^2} - \rho_l \frac{\partial^2 \beta}{\partial t^2}. \quad (20)$$

Setting the pressure field p as a mono-harmonic wave:

$$p(\mathbf{r}, t) = \frac{1}{2} \left(P(\mathbf{r}) e^{i\omega t} + \overline{P}(\mathbf{r}) e^{-i\omega t} \right),$$

the linearization of the above equation and of the bubble dynamics equation allows to show that the complex field P fulfills an Helmholtz equation:

$$\nabla^2 P + k^2 P = 0,$$

where the complex wave number is given by the linear dispersion relation [17, 20, 23, 28, 32]:

$$k^2 = \frac{\omega^2}{c_l^2} + \frac{4\pi R_0 \omega^2 N}{\omega_0^2 - \omega^2 + 2ib\omega}. \quad (21)$$

In Eq. (21), ω_0 is the resonance frequency and b the damping factor, respectively given by

$$\omega_0^2 = \frac{p_0}{\rho R_0^2} [(1+S)\Re(\Phi_g) - S], \quad (22)$$

$$2b = \frac{p_0(1+S)}{\rho \omega R_0^2} \Im(\Phi_g) + \frac{4\mu_l}{\rho R_0^2}. \quad (23)$$

It can be readily seen, that, even for sub-resonant bubbles ($\omega < \omega_0$), the wave number is complex because of the damping factor b , which, as expected from the discussion in Sec. 2.3, is correlated with the heat loss from the bubble and the viscous friction in the liquid. The imaginary part of the wave number represents the attenuation factor of the wave, and can be easily calculated by setting $k = k_r - i\alpha$ and identifying k_r and α from Eq. (21).

Generalizing this simple theory for inertial cavitation sounds unrealistic, since the bubble dynamics cannot be reasonably linearized for inertial oscillations. Thus all the fields are not mono-harmonic anymore and the problem cannot be reduced to an Helmholtz equation. However, for periodic oscillations, either linear or not, the correlation between the energy dissipated by each bubble over one cycle and the attenuation of the wave remains a universal principle, formalized by Eq. (8), and constitutes the guideline of the following derivation.

We will therefore show that the first harmonic component of the field (at the frequency ω of the driving) approximately follows an Helmholtz equation, but whose wave number is directly expressed as functions of the dissipation functions Π_{th} and Π_v presented in the precedent section. This procedure allows to generalize the linear model, in the sense that the time-variable is eliminated, but keeping realistic values for the energy dissipated by inertial bubbles.

3.2. Derivation of the model

We decompose the pressure field into a sum of a time-average pressure p_m , a first harmonic pressure p_1 , oscillating at the frequency of the ultrasonic source, and harmonic terms noted p_{osc} , that could be written as a Fourier series starting with a term at the frequency 2ω :¹

$$p(\mathbf{r}, t) = p_m(\mathbf{r}) + p_1(\mathbf{r}, t) + p_{osc}(\mathbf{r}, t). \quad (24)$$

The first harmonic pressure field p_1 is expressed as:

$$p_1(\mathbf{r}, t) = \frac{1}{2} \left(P(\mathbf{r}) e^{i\omega t} + \overline{P}(\mathbf{r}) e^{-i\omega t} \right), \quad (25)$$

where over-lines denote complex conjugate. Next, we set w the primitive of the first harmonic pressure field:

$$w = \frac{1}{2} \frac{1}{i\omega} \left(P(\mathbf{r}) e^{i\omega t} - \overline{P}(\mathbf{r}) e^{-i\omega t} \right). \quad (26)$$

¹We assume here for simplicity that there is no subharmonics or ultra-harmonic terms, but the following reasoning can always be generalized by taking time-averages over the largest period of the pressure field.

Multiplicating the propagation equation (20) by w and averaging over one acoustic period yields:

$$\langle w \nabla^2 p \rangle = \frac{1}{c_l^2} \left\langle w \frac{\partial^2 p}{\partial t^2} \right\rangle - \rho_l \left\langle w \frac{\partial^2 \beta}{\partial t^2} \right\rangle. \quad (27)$$

Integrating by parts, using the definition of w , and the fact that all quantities are periodic, we obtain:

$$\langle w \nabla^2 p \rangle = -\frac{1}{c_l^2} \left\langle p_1 \frac{\partial p}{\partial t} \right\rangle + \rho_l \left\langle p_1 \frac{\partial \beta}{\partial t} \right\rangle. \quad (28)$$

Using the decomposition (24), it can be easily seen that $\langle w \nabla^2 p \rangle = \langle w \nabla^2 p_1 \rangle$ and that $\langle p_1 \partial p / \partial t \rangle = 0$. Besides, using Eq. (24), the second term of the right-hand-side of (28) can be expressed as:

$$\left\langle p_1 \frac{\partial \beta}{\partial t} \right\rangle = \left\langle p \frac{\partial \beta}{\partial t} \right\rangle - \left\langle p_{osc} \frac{\partial \beta}{\partial t} \right\rangle,$$

since $\langle p_m \partial \beta / \partial t \rangle = p_m \langle \partial \beta / \partial t \rangle = 0$. We now make the empirical assumption that $\langle p_{osc} \partial \beta / \partial t \rangle$ is negligible. A rigorous justification for this assumption is difficult in absence of results on the respective orders of magnitude of p_1 and p_{osc} . However, unpublished measurements show that the latter is generally one order of magnitude lower than the former, so that for now, we assume that the assumption is justified. We therefore conclude that:

$$\left\langle p_1 \frac{\partial \beta}{\partial t} \right\rangle \simeq \left\langle p \frac{\partial \beta}{\partial t} \right\rangle \quad (29)$$

A physical interpretation of this approximate equation can be given by looking at Eqs. (4), (7): it reverts to consider that the interaction between the acoustic field and the bubbles only occur through the first harmonic part of the field, and that the bubble mainly responds to this first harmonic content. We will term this hypothesis as “first harmonic approximation” (FHA). From this assumption and the above derivation, Eq. (28) takes therefore the approximate form:

$$\langle w \nabla^2 p_1 \rangle = \rho_l \left\langle p \frac{\partial \beta}{\partial t} \right\rangle, \quad (30)$$

and using Eq. (8), Eq. (30), we finally obtain:

$$\langle w \nabla^2 p_1 \rangle = -N (\Pi_{th} + \Pi_v). \quad (31)$$

We can now use the harmonic expressions (25) and (26) of p_1 and w , to obtain:

$$\frac{i}{4\omega} (\overline{P} \nabla^2 P - P \nabla^2 \overline{P}) = -\rho_l N (\Pi_{th} + \Pi_v),$$

and, dividing both sides of this equation by $|P|^2$, P is finally found to fulfill:

$$\Im \left(\frac{\nabla^2 P}{P} \right) = 2\rho_l \omega N \frac{\Pi_{th} + \Pi_v}{|P|^2}, \quad (32)$$

where \Im denotes the imaginary part. We therefore see that if P were to fulfill an Helmholtz equation, the wave number would necessarily satisfy following relation:

$$\Im(k^2) = -2\rho_l\omega N \frac{\Pi_{th} + \Pi_v}{|P|^2}. \quad (33)$$

This equation is a generalization of the linear case represented by Eq. (21), but here, Π_{th} and Π_v can be estimated from fully nonlinear bubble dynamics. By the way, it can be checked after a few algebra that, linearizing Π_{th} and Π_v , Eq. (33) yields the same results as taking the imaginary part of the dispersion relation (21). For linear oscillations, Π_{th} and Π_v scale as $|P|^2$ (see left part of the curves in Figs. 1 and 2), so that linear theory yields a value of $\Im(k^2)$ independent of the driving amplitude $|P|$. This is no longer the case for nonlinear oscillations and Eq. (33) yields a value of $\Im(k^2)$, which now depends on the local magnitude of the acoustic pressure $|P|$.

The idea of the present paper is thus to use Eq. (33) by using the nonlinear values of Π_{th} and Π_v obtained in Sec. 2.3 to calculate $\Im(k^2)$, and, relying on Eq. (32), to introduce the latter in a nonlinear Helmholtz equation:

$$\nabla^2 P + k^2(|P|)P = 0. \quad (34)$$

Clearly, owing to the approximations made above, some additional terms would appear in the exact equation fulfilled by P . However, Eq. (33) has the advantage to clearly link the attenuation factor to the real dissipation of energy by the bubbles. Since it only yields the imaginary part of k^2 , there remains the problem of calculating its real part. For now, we still use the linear dispersion relation to evaluate $\Re(k^2)$, and defer the discussion of this approximation below:

$$\Re(k^2) = \frac{\omega^2}{c_l^2} + \frac{4\pi R_0 \omega^2 N}{\omega_0^2 - \omega^2}. \quad (35)$$

The attenuation coefficient and the real part of the wave number can now be deduced from:

$$k = k_r - i\alpha, \quad (36)$$

and by identification with (33)-(35).

Figure 4 displays the attenuation coefficient α calculated by following this procedure (thick solid line), for $5\ \mu\text{m}$ bubbles, and a typical [59] void fraction $\beta_0 = 5 \times 10^{-5}$, as a function of the acoustic pressure $|P|$. The attenuation coefficient rises abruptly for acoustic pressures just above the Blake threshold, as do Π_{th} and Π_v , and becomes about 4 orders of magnitude larger than its linear value [thin solid line, calculated from Eq. (21)]. This demonstrates that a cloud of inertial cavitation bubbles damps out the incident wave much more drastically than linearly oscillating bubbles. Moreover, contrarily to the linear prediction, the attenuation coefficient increases with the wave peak-amplitude. Thus, increasing the source vibration amplitude does not necessarily produce a more extended bubble

field since increasing the acoustic pressure also increases the attenuation. This self-saturation phenomenon is well-known in cavitation experiments [36], and will be demonstrated in the simulations of the next section.

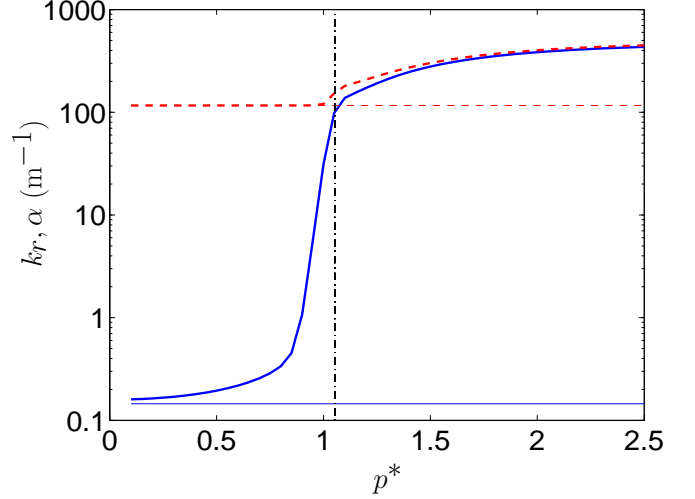


Figure 4: Real part (dashed) and imaginary part (solid) of the wave number k . The thin horizontal lines are predictions from linear theory (21) and the thick lines are results calculated from Eqs. (33), (35). The vertical dash-dotted line represents the Blake threshold.

The real part of the wave number is also displayed in Fig. 4 (thick dashed line), and the constant linear value predicted by (21) is recalled (thin dashed line) for comparison. It is interesting to note that, above the Blake threshold, k_r closely follows α . This comes from the fact that the imaginary part of k^2 , calculated from the dissipation functions by Eq. (33), is much larger in absolute value than its real part (35). This can be seen by writing the complex wave number as:

$$k^2 = K^2 \exp[i(\epsilon - \pi/2)], \quad (37)$$

where ϵ is a small number, since $\Im(k^2)$ is negative and large. The wave number k therefore reads:

$$k = K \exp[i(\epsilon/2 - \pi/4)], \quad (38)$$

and is therefore almost equal to $K(1 - i)/\sqrt{2}$, so that we indeed have $k_r \simeq \alpha$.

The ratio α/k_r has a strong physical sense. The attenuation of the wave over one wavelength λ is $\exp(-\alpha\lambda) = \exp(-2\pi\alpha/k_r)$. Thus, if as in the present case α is of the same order of magnitude as k_r , the attenuation of the wave over one wavelength is of the order of $\exp(-2\pi) \simeq 0.002$. This means that as soon as the imaginary part of k^2 is much larger than its real part, attenuation will play a dominant role whatever the precise value of its real value. This is why the precise choice of $\Re(k^2)$ is of minor importance, and Eq. (35) is a good compromise.

4. Results

4.1. 1D wave profiles

We consider a tube of length L filled with water, bounded on the left by a piston which oscillating displacement reads:

$$U(t) = U_0 \cos \omega t \quad (39)$$

and on the right by an infinitely soft boundary, imposing a zero acoustic pressure. This arbitrary boundary condition was chosen so that a standing wave should be obtained in the absence of bubbles. It can be easily changed to different and more complex conditions, as will be exemplified in the companion paper.

We consider $5 \mu\text{m}$ air bubbles. This choice is partially justified by experimental measurements of bubble size distributions at low frequency [9, 59]. In order to solve (34) along with Eqs. (33)-(35), the bubble density N must be known. For now, we consider that bubbles are only present in the zones where the acoustic pressure amplitude is above the Blake threshold Eq. (6), and with a uniform density:

$$N = \begin{cases} N_0 & \text{if } |P| > P_B \\ 0 & \text{if } |P| < P_B \end{cases} \quad (40)$$

The nonlinear Helmholtz equation along with (40) and the above boundary conditions is solved using the commercial COMSOL software, and a mesh convergence was performed.

Figure 5 displays the profiles of the peak acoustic pressure $|P^*| = P/p_0$ obtained for various amplitude of the source. For the smallest amplitude of the emitter $U_0 = 0.2 \mu\text{m}$, we recover a standing wave profiles in the pure liquid (dash-dotted line). For a slightly larger vibration of the emitter $U_0 = 0.5 \mu\text{m}$ (dashed line), the acoustic pressure at the antinodes is just above the Blake threshold, so that the bubbles present here start to dissipate some energy. This yields nonzero acoustic pressures at the nodes, but the profile remains globally similar to a linear standing wave profile. When the amplitude of the source is much larger ($U_0 = 5 \mu\text{m}$, solid line), the wave profile completely changes, and is drastically attenuated in a zone of about 1 cm width near the emitter. This is due to the fact that the acoustic pressure near the emitter is larger than the Blake threshold, so that the bubbles present in this zone dissipate a lot energy. The remaining part of the profile is similar to a damped linear standing wave.

In order to emphasize the importance of the nonlinear energy dissipation accounted for by our model, we present in Fig. 6 a comparison of the upper profile of Fig. 5 ($U_0 = 5 \mu\text{m}$, thick solid line), to the profile that would be obtained either by using the linear relation dispersion (21) with the same bubble density (thin solid line), or in the pure liquid (thin dashed line). The important conclusion is that the two linear models predict unrealistic huge values of the acoustic pressure, while our model yields commonly measured amplitudes at 20 kHz (typically 1.5-3 bar [9]).

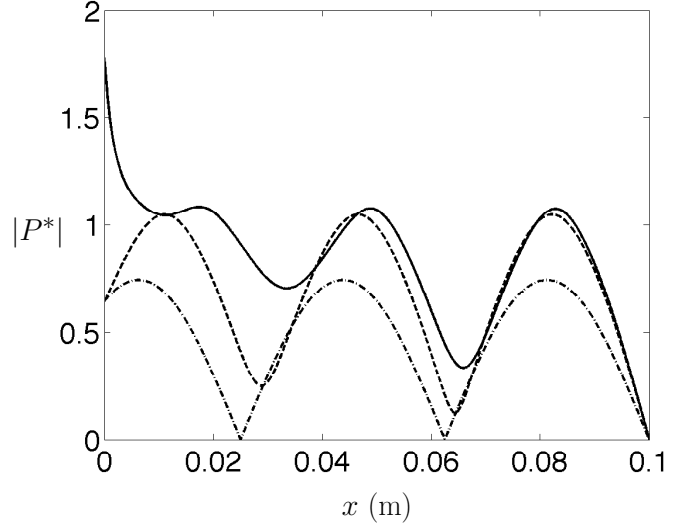


Figure 5: Peak value of the dimensionless pressure field, calculated by solving numerically Eq. (34) for various emitter displacement amplitudes. Solid line: $U_0 = 5 \mu\text{m}$; dashed line: $U_0 = 0.5 \mu\text{m}$; dash-dotted line: $U_0 = 0.2 \mu\text{m}$.

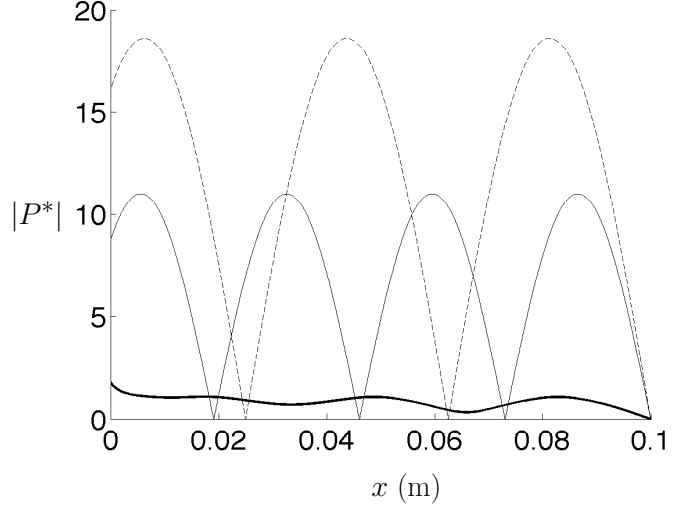


Figure 6: Wave profiles for an amplitude of the emitter of $5 \mu\text{m}$. Thick solid curve: predicted by the present model (same as the thick solid curve of Fig. 5); thin solid curve: obtained by the linear dispersion relation Eq. (21); thin dashed curve: obtained in the pure liquid.

4.2. Standing and traveling waves

The phase θ between the pressure field and the pressure gradient allows to determine whether the wave is traveling or standing. For a purely traveling wave (typically $p(x, t) \sim e^{i(\omega t - kx)}$), pressure and pressure gradient are in phase quadrature, so that $|\sin \theta| = 1$. Conversely, for a purely standing wave (typically $p(x, t) \sim \cos(kx)e^{i\omega t}$), pressure and pressure gradient are in phase or in phase opposition, so that $|\sin \theta| = 0$ in the latter case [60]. Thus, the quantity $\sin^2 \theta$ can be used as a measurement of the

traveling character of the wave.

In the configuration studied here, where the domain is closed with perfectly reflecting boundaries, linear acoustics without dissipation would predict a perfect standing wave. However, if there is attenuation in the medium, a traveling wave component appears, because the reflected wave is of lower amplitude than the incident wave. This can be checked on Fig. 7, where $\sin^2 \theta$ is displayed for the same simulation conditions as Fig. 5. It is seen that for low driving amplitudes ($U_0 = 0.2 \mu\text{m}$, dash-dotted line), $\sin^2 \theta$ is 0 everywhere, so that we have an almost perfect standing wave (which was clearly visible on Fig. 5). But for higher emitter amplitude ($U_0 = 0.5 \mu\text{m}$, dashed line), $\sin^2 \theta$ starts to increase everywhere in the medium, especially near the pressure antinodes, and for $U_0 = 5 \mu\text{m}$ (solid line), $\sin^2 \theta$ progressively increases toward 1 in a large part of the medium.

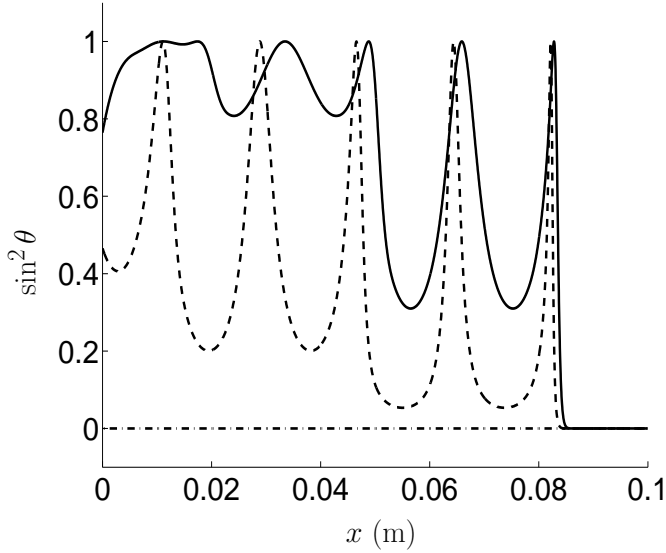


Figure 7: Phase between pressure and pressure gradient in the same conditions as Fig. 5. The line-styles are the same as for Fig. 5

Finally, Fig. 8 confirms that, as shown above [see Eq. (38)], the phase of the complex wave number k is close to $-\pi/4$ in zones where the bubbles oscillate inertially. The wave number k is thus proportional to $1 - i$, which means that the attenuation factor α and the real part k_r of the wave number are of the same orders of magnitude.

5. Conclusion

Inertial bubbles dissipate much more energy than a linearly oscillating bubble, both by thermal diffusion in the gas and viscous dissipation in the liquid, the latter mechanism being dominant for bubble ambient radii lower than $10 \mu\text{m}$. The wave attenuation in an inertial cavitation field is therefore much larger than the value predicted by the classical linear dispersion relation (by typically 4 orders

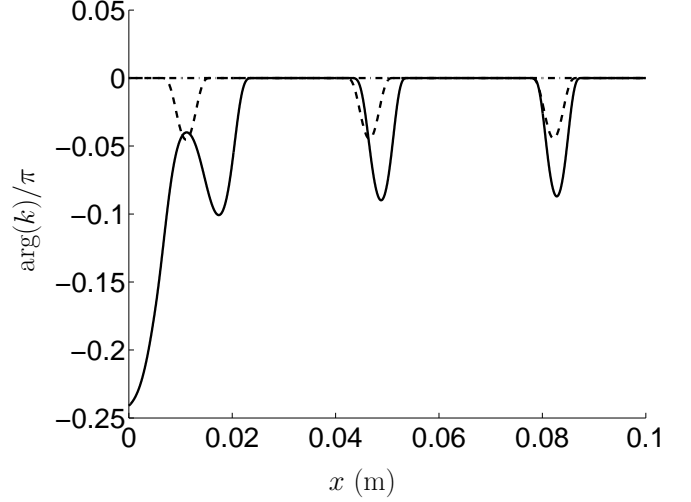


Figure 8: Phase of the complex wave number k divided by π , in the same conditions as Fig. 5, for $U_0 = 5 \mu\text{m}$ (solid line) $U_0 = 0.5 \mu\text{m}$ (dashed line), and $U_0 = 0.2 \mu\text{m}$ (dash-dotted line). For the largest amplitude, the wave number near the emitter is seen to approach $-\pi/4$, as expected from Eq. (38).

of magnitude). Although the latter conclusion is qualitatively intuitive, to our knowledge, no quantitative estimation has ever been reported.

Under the assumption that the bubbles are mainly excited by the first harmonic content of the acoustic field, the latter fulfills approximately a nonlinear Helmholtz equation. The imaginary part of the squared wave number is estimated rigorously from the energy dissipated by a single bubble, which can be easily calculated by solving a bubble dynamic equation. The real part is still arbitrarily estimated from the linear theory, but this arbitrary choice was shown to be of low importance, owing to the huge value of the imaginary part. This has the importance consequence that in bubbly zones, the attenuation factor is of the same order of magnitude as the real part of the wave number, which results in a strong attenuation of the wave.

The model has been solved in a typical 1D-domain, and yields as expected a strongly attenuated wave profile near the emitter for high amplitude vibrations of the latter. The amplitude of the calculated acoustic pressure fields are realistic, contrarily to linear theory. This strong attenuation yields in turn a traveling component in the wave, where purely standing waves would be expected in a non dissipative medium enclosed by perfectly reflecting boundaries.

It is interesting to note that following the present results, attenuation, and therefore wave structures, are mainly governed by viscous dissipation involved in the bubble radial motion, the thermal effects in the bubble playing a minor role. This conjecture might be checked experimentally by measuring the wave attenuation for solutions of different viscosities and with different dissolved gas.

The choice of the incompressible Rayleigh-Plesset equation to model the bubble dynamics may be questioned.

Although this is the original formulation of the Caffish model, the compressibility of the liquid produces sound scattering, and contributes therefore to the attenuation of waves in bubbly liquids, as is well-known in the linear case [17, 20]. One may therefore replace Eq. (5) for example by a Keller equation [61–63], and reformulate the energy equation (8) to exhibit an additional contribution of radiation Π_a in its right-hand-side. This would in turn add a contribution in Eq. (33), and produce more wave attenuation. However, the procedure is not straightforward, and the energetical interpretation in this case is less easy. One of the reasons for that is that compressible bubble dynamics equations are not exact solutions of the basic physical principles [62, 63], but only first terms of expansions in the parameter \dot{R}/c_l . It is also expected that sound scattering also modifies the real part of k^2 , which again raises the issue of a correct expression for the latter. However, it may be conjectured that, in the low frequency range studied here, the power loss by sound scattering is much lower than the one produced by viscous dissipation, because, as for thermal effects, sound radiation occurs mainly in the vicinity of the collapse. Thus we expect that the model in its present form catches the main dissipation phenomenon and that the values proposed for $\Im(k^2)$ is a good estimation. This will be examined in more details in future work.

The occurrence of traveling waves, aside of the issue of the Bjerknes forces examined in the companion paper, may also have fundamental consequences on the final stage of the bubbles collapse. Indeed, it has been shown recently that bubbles in traveling waves are more exposed to shape instabilities and can undergo jetting, which reduces the final collapse temperature [64], compared to a spherically collapsing bubble. This would therefore influence the estimation of the heat lost by a single bubble, but the spherical collapse model used in the present study yields an upper value.

Besides, measurements of the acoustic field in conical structures has revealed the presence of a time-independent mean pressure field, which amplitude may be comparable with the first-harmonic part [36]. Our model does not catch this feature, and there is yet no correct theoretical description of this phenomenon. We emphasize however that our derivation of the imaginary part of the wave number is valid even in this case, since our decomposition of the field Eq. (24) accounts a priori for the presence of such a mean field. This suggests that the present model could be supplemented by a specific equation describing this mean pressure field, which remains to be determined.

To conclude, we believe that the present model opens the way to more realistic simulations of the coupled evolution of the cavitation field and the acoustic field. The nonlinear Helmholtz equation is relatively easy to solve and constitutes a viable solution halfway between a fully nonlinear simulation of the Caffish equations, which requires painful, if not intractable, temporal integration, and a fully linearized model which, as shown above, yields unrealistic acoustic pressure values. The companion paper

will address the calculation of the Bjerknes forces in the acoustic fields calculated with the present model, and the resulting bubble structures predicted in more complex 2D configurations.

6. Acknowledgments

The author acknowledges the support of the French Agence Nationale de la Recherche (ANR), under grant SONONUCLICE (ANR-09-BLAN-0040-02) "Contrôle par ultrasons de la nucléation de la glace pour l'optimisation des procédés de congélation et de lyophilisation". Besides the author would like to thank Nicolas Huc of COMSOL France for his help in solving convergence issues.

References

- [1] S. Hilgenfeldt, D. Lohse, M. P. Brenner, *Phys. Fluids* 8 (11) (1996) 2808–2826.
- [2] Y. Hao, A. Prosperetti, *Phys. Fluids* 11 (6) (1999) 1309–1317.
- [3] L. Yuan, C. Y. Ho, M. C. Chu, P. T. Leung, *Phys. Rev. E* 64 (016317) (2001) 1–6.
- [4] B. D. Storey, *Phys. Rev. E* 64 (2001) 017301–017301–3.
- [5] M. P. Brenner, S. Hilgenfeldt, D. Lohse, *Rev. Mod. Phys.* 74 (2) (2002) 425–483.
- [6] H. Lin, B. D. Storey, A. J. Szeri, *Phys. Fluids* 14 (8) (2002) 2925–2928.
- [7] R. Mettin, in: T. Kurz, U. Parlitz, U. Kaatz (Eds.), *Oscillations, Waves and Interactions*, Universitätsverlag Göttingen, 2007, pp. 171–198.
- [8] R. G. Holt, D. F. Gaitan, *Phys. Rev. Lett.* 77 (1996) 3791–3794.
- [9] R. Mettin, in: A. A. Doinikov (Ed.), *Bubble and Particle Dynamics in Acoustic Fields: Modern Trends and Applications*, Research Signpost, Kerala (India), 2005, pp. 1–36.
- [10] R. Mettin, J. Appel, D. Krefting, R. Geisler, P. Koch, W. Lauterborn, in: *Special Issue of the Revista de Acustica, Forum Acusticum Sevilla, Spain, 16–20 Sept. 2002, Vol. XXXIII*, Sevilla, Spain, 2002, pp. 1–4.
- [11] R. Mettin, P. Koch, D. Krefting, W. Lauterborn, in: O. V. Rudenko, O. A. Sapozhnikov (Eds.), *Nonlinear Acoustics at the Beginning of the 21st Century*, (Proceedings of the 16th International Symposium on Nonlinear Acoustics ISNA-16), Vol. 2, Faculty of Physics, MSU, Moscow, 2002, 2006, pp. 1003–1006.
- [12] A. Moussatov, C. Granger, B. Dubus, *Ultrasonics Sonochemistry* 10 (2003) 191–195.
- [13] J. Appel, P. Koch, R. Mettin, W. Lauterborn, *Ultrasonics Sonochemistry* 11 (2004) 39–42.
- [14] I. Akhatov, R. Mettin, C. D. Ohl, U. Parlitz, W. Lauterborn, *Phys. Rev. E* 55 (3) (1997) 3747–3750.
- [15] R. Mettin, I. Akhatov, U. Parlitz, C. D. Ohl, W. Lauterborn, *Phys. Rev. E* 56 (3) (1997) 2924–2931.
- [16] U. Parlitz, R. Mettin, S. Luther, I. Akhatov, M. Voss, W. Lauterborn, *Phil. Trans. R. Soc. Lond. A* 357 (1999) 313–334.
- [17] L. L. Foldy, *Phys. Rev.* 67 (3-4) (1944) 107–119.
- [18] E. L. Carstensen, L. L. Foldy, *J. Acoust. Soc. Am.* 19 (3) (1947) 481–501.
- [19] P. M. Morse, H. Feshbach, *Methods of theoretical physics*, McGraw-Hill, 1953.
- [20] K. W. Commander, A. Prosperetti, *J. Acoust. Soc. Am.* 85 (2) (1989) 732–746.
- [21] A. Prosperetti, in: S. Morioka, L. van Wijngaarden (Eds.), *IUTAM Symposium on waves in liquid/gas and liquid/vapour two-phase systems*, Kluwer Academic Publishers, 1995, pp. 55–65.
- [22] S. Iordansky, *J. Appl. Mech. Tech. Phys.* 3 (1960) 102–110.
- [23] L. van Wijngaarden, in: *6th Symposium on Naval Hydrodynamics*, Office of Naval Research, Washington DC, 1966, pp. 115–128.
- [24] L. van Wijngaarden, *J. Fluid Mech.* 33 (3) (1968) 465–474.
- [25] G. B. Whitham, *Linear and nonlinear waves*, Wiley-Interscience, 1974.
- [26] L. van Wijngaarden, *Ann. Rev. Fluid Mech.* 4 (1972) 369–396.
- [27] V. V. Kuznetsov, V. E. Nakoriakov, B. G. Pokusaev, I. R. Schreiber, *JETP Lett.* 23 (1976) 172–176.
- [28] A. Prosperetti, *J. Fluid. Mech.* 222 (1991) 587–616.
- [29] L. Noordzij, L. van Wijngaarden, *J. Fluid Mech.* 66 (1) (1972) 115–143.
- [30] V. V. Kuznetsov, V. E. Nakoriakov, B. G. Pokusaev, I. R. Schreiber, *J. Fluid Mech.* 85 (1978) 85–96.
- [31] L. van Wijngaarden, *Acta Applicandae Mathematicae* 39 (1995) 507–516.
- [32] R. E. Caflish, M. J. Miksis, G. C. Papanicolaou, L. Ting, *J. Fluid Mech.* 153 (1985) 259–273.
- [33] Y. A. Kobelev, L. A. Ostrovskii, *J. Acoust. Soc. Am.* 85 (2) (1989) 621–629.
- [34] I. Akhatov, U. Parlitz, W. Lauterborn, *J. Acoust. Soc. Am.* 96 (6) (1994) 3627–3635.
- [35] E. Silberman, *J. Acoust. Soc. Am.* 29 (8) (1957) 925–933.
- [36] C. Campos-Pozuelo, C. Granger, C. Vanhille, A. Moussatov, B. Dubus, *Ultrasonics Sonochemistry* 12 (2005) 79–84.
- [37] S. Dähnke, K. M. Swamy, F. J. Keil, *Ultrasonics Sonochemistry* 6 (1999) 31–41.
- [38] S. Dähnke, K. M. Swamy, F. J. Keil, *Ultrasonics Sonochemistry* 6 (4) (1999) 221 – 226.
- [39] G. Servant, J. L. Laborde, A. Hita, J. P. Caltagirone, A. Gérard, *Ultrasonics Sonochemistry* 10 (6) (2003) 347–355.
- [40] R. Mettin, P. Koch, W. Lauterborn, D. Krefting, in: *Sixth International Symposium on Cavitation - CAV2006* (paper 75), Wageningen (The Netherlands), 2006, pp. 125–129.
- [41] L. D. Rozenberg, in: L. D. Rozenberg (Ed.), *High-intensity ultrasonic fields*, Plenum Press, New-York, 1971.
- [42] O. Louisnard, *Contribution à l'étude de la propagation des ultrasons en milieu cavitant*, Thèse de doctorat, Ecole des Mines de Paris (1998).
- [43] C. Vanhille, C. Campos-Pozuelo, *Ultrasonics Sonochemistry* 16 (2009) 669–685.
- [44] O. Louisnard, *Physics Procedia* 3 (1) (2010) 735 – 742, international Congress on Ultrasonics, Santiago de Chile, January 2009.
- [45] I. Akhatov, N. Gumerov, C. D. Ohl, U. Parlitz, W. Lauterborn, *Phys. Rev. Lett.* 78 (2) (1997) 227–230.
- [46] S. Hilgenfeldt, M. P. Brenner, S. Grossman, D. Lohse, *J. Fluid Mech.* 365 (1998) 171–204.
- [47] O. Louisnard, F. Gomez, *Phys. Rev. E* 67 (3) (2003) 036610.
- [48] O. Louisnard, *Phys. Rev. E* 78 (3) (2008) 036322.
- [49] T. J. Matula, *Philos. Trans. R. Soc. London, Ser. A* 357 (1999) 225–249.
- [50] O. Louisnard, In preparation .
- [51] R. Toegel, B. Gompf, R. Pecha, D. Lohse, *Phys. Rev. Lett.* 85 (15) (2000) 3165–3168.
- [52] B. D. Storey, A. Szeri, *Proc. R. Soc. London, Ser. A* 457 (2001) 1685–1700.
- [53] T. J. Matula, P. R. Hilmo, B. D. Storey, A. J. Szeri, *Phys. Fluids* 14 (3) (2002) 913–921.
- [54] J. C. Devin, *J. Acoust. Soc. Am.* 31 (12) (1959) 1654–1667.
- [55] A. Prosperetti, *J. Acoust. Soc. Am.* 61 (1) (1977) 17–27.
- [56] A. Prosperetti, L. A. Crum, K. W. Commander, *J. Acoust. Soc. Am.* 83 (1988) 502–514.
- [57] D. F. Gaitan, R. G. Holt, *Phys. Rev. E* 59 (1999) 5495–5502.
- [58] O. Louisnard, J. Gonzalez-Garcia, I. Tudela, J. Klima, V. Saez, Y. Vargas-Hernandez, *Ultrasonics Sonochemistry* 16 (2009) 250–259.
- [59] F. Burdin, N. A. Tsochatzidis, P. Guiraud, A. M. Wilhelm, H. Delmas, *Ultrasonics Sonochemistry* 6 (1999) 43–51.
- [60] P. M. Morse, K. U. Ingard, *Theoretical acoustics*, McGraw-Hill, 1968.
- [61] J. B. Keller, M. Miksis, *J. Acoust. Soc. Am.* 68 (1980) 628–633.
- [62] A. Prosperetti, A. Lezzi, *J. Fluid Mech.* 168 (1986) 457–478.
- [63] A. A. Doinikov, *Recent Res. Devel. Acoustics* 2 (2005) 13–38.
- [64] M. L. Calvisi, O. Lindau, J. R. Blake, A. J. Szeri, *Physics of Fluids* 19 (4) (2007) 047101–4.

List of Figures

1	Dimensionless power dissipated by an argon bubble of ambient radius $R_0 = 3 \mu\text{m}$ in water, at 20 kHz: by viscosity Π_v^* [thick solid line, from Eq. (13)]; by thermal diffusion, Π_{th}^* [thick dashed line, from Eq (12)]. The thin lines are the corresponding values obtained from linear theory, Eqs. (15)-(16) (solid: $\Pi_{v,lin}^*$; dashed: $\Pi_{th,lin}^*$). The vertical dash-dotted line represents the Blake threshold calculated by Eq. (6)	5
2	Same as Fig. 1 for a $8 \mu\text{m}$ bubble.	5
3	Same as Figs. 1 and 2, but varying R_0 for $P^* = 1.5$. The vertical dash-dotted line represents the Blake threshold.	6
4	Real part (dashed) and imaginary part (solid) of the wave number k . The thin horizontal lines are predictions from linear theory (21) and the thick lines are results calculated from Eqs. (33), (35). The vertical dash-dotted line represents the Blake threshold.	8
5	Peak value of the dimensionless pressure field, calculated by solving numerically Eq. (34) for various emitter displacement amplitudes. Solid line: $U_0 = 5 \mu\text{m}$; dashed line: $U_0 = 0.5 \mu\text{m}$; dash-dotted line: $U_0 = 0.2 \mu\text{m}$	9
6	Wave profiles for an amplitude of the emitter of $5 \mu\text{m}$. Thick solid curve: predicted by the present model (same as the thick solid curve of Fig. 5); thin solid curve: obtained by the linear dispersion relation Eq. (21); thin dashed curve: obtained in the pure liquid.	9
7	Phase between pressure and pressure gradient in the same conditions as Fig. 5. The line-styles are the same as for Fig. 5	10
8	Phase of the complex wave number k divided by π , in the same conditions as Fig. 5, for $U_0 = 5 \mu\text{m}$ (solid line) $U_0 = 0.5 \mu\text{m}$ (dashed line), and $U_0 = 0.2 \mu\text{m}$ (dash-dotted line). For the largest amplitude, the wave number near the emitter is seen to approach $-\pi/4$, as expected from Eq. (38).	10